CrossMark

Cooling enhancement of planar-balanced magnetron cathode

M'hamed Salhi[1,2] · Seddik El Hak Abaidia[2] · Brahim Mohamedi[1] ·
Sofiane Laouar[1]

Abstract In physical vapor deposition on a magnetron
cathode, temperature of sensitive components must be kept
under threshold limit, so as to ensure the cathode reliability,
the process reproducibility, and the best quality of thin films.
This can be achieved by an adequate design to enhance the
dissipation of heat generated at the cathode. In this paper,
temperature distribution and streamlines velocity of the
cathode coolant inside a cathode magnetron are analyzed by
using CFD solver ANSYS FLUENT in the single-phase
method in combination with k–ε standards turbulent model.
The results show that the design is appropriate under the
calculation parameters, and for high heat densities some
improvements are necessary to enhance heat dissipation and
keep temperature under the threshold limit.

Keywords Magnetron cathode · PVD · Temperature
threshold · CFD · ANSYS FLUENT

1 Introduction

Magnetron sputtering configuration (MSC) is a common
method in physical vapor deposition (PVD) processes for a
wide range of industrial coatings. It allows obtaining high-
quality functional thin films with appropriate reproducible
properties [1, 2]. Under a magnetic field and an oscillating
electric field, electrons generated in glow-discharge plasma
per ions bombardment of target surface (cathode) follow a
spiral closed path and are maintained close to the cathode
surface. This high flux of electrons creates high-density
plasma and high temperature [3] by means of electron-
atom collisions and ionization. This, in turn, leads to higher
sputtering rates and, therefore, higher deposition rates at
the substrate (anode). The main factors limiting the depo-
sition rate are thermal conductance of the target, efficiency
of the cathode cooling, melting point of the target, and the
sputtering yield [4].

Among MSCs of different types, the planar-balanced or
unbalanced magnetron source is the simplest and commonly
used [5–9]. An excessive local heating of the principal
components (namely the target and magnets), under effect of
the delivered power, can take place if the heat dissipation and
thermal contact between the components are not suitable.
Without an adequate cooling of the cathode, structures of the
magnets can be affected by overheating (over the Curie
temperature), resulting in a disorder of the uniform distribu-
tion of the field lines and consequently the deviation of the
trajectories of plasma electrons occurs. On top of that, the
erosion of the target may occur in a non-uniform manner [10].

Kelly and Arnell [2] reported that the target could reach a
local temperature of 400 °C which could damage the target
and magnets. Lake and Harding [11] designed an adequate
cooling system to ensure a good heat dissipation and a better
thermal compatibility between the mechanical components
of the magnetron source. Takatsuji et al. [12] found that the
flow rate of target cooling in a DC magnetron sputtering
affected greatly the crystalline structure of deposited alu-
minum film, with a low texture in (111) orientation at low

✉ M'hamed Salhi
  mn_salhi@yahoo.fr

1 Centre de Recherche Nucléaire de Birine, B.P. 180,
   17200 Ain-Oussera, Algeria

2 Unité de Recherche MPE, Faculté des Sciences de
   l'Ingénieur, Université M'hamed Bougarra de Boumerdès,
   35000 Boumerdès, Algeria

flow rate, and at low flow rate of cooling the high-temperature cathode caused a transformation of certain components and degassing of the sputtering chamber walls. Baek and Kim [13] used two shapes of cooling water path in rectangular magnetron source for enhancing heat dissipation of the target. Doerner et al. [14] found that whatever the magnetic properties of magnets, an over-threshold temperature increase in the cathode often led to an increase in deposition rate; consequently, the sputtering of cathode atoms becomes uncontrolled and the deposited films are not in desired quality. Recently Caillard et al. [15] used the calorimetric method to study the energy transfer to the substrate during a cathode magnetron sputtering of a pure nickel target and showed that the rate of pulverization and the coefficient of secondary ion emission increased at the Curie temperature ($T_C = 358\ °C$). From this temperature threshold, the discharge illuminates in visible and infrared ranges.

The present paper is concerned with computational fluid dynamic (CFD) to study magnetron cathode (MC). The focus is placed on the numerical simulation of the preconditioning of single-phase flows in an annular path target cooling, titanium or nickel as appropriate, under heated wall conditions, with the target being a heat source of the magnetron cathode. CFD technique shows increasing promise for simulating vapor deposition processes. The commercial CFD solver ANSYS FLUENT is employed as the computational platform, and the single-phase method in combination with standard k–ε turbulent model is used. This model is the most general among all the models of flow.

2 Overview of the magnetron cathode design

A planar-balanced magnetron cathode was designed at UR-MPE of Boumerdes University with the contribution of Nuclear Research Centre of Birine, in order to build a PVD bi-cathode magnetron system [16]. The cathode has a plane circular geometry with outer diameter of 90 mm (Fig. 1). NdFeB magnets with magnetic field of 400 mT intensity are arranged in such a way that one pole is positioned at the target central axis and the second pole is formed by a ring of magnets around the target outer edge. Targets of $\Phi 50$ mm are fixed tightly at the upper side of magnets, and a 3-mm soft iron, as magnetic yoke, is placed at the lower side of the magnets in order to confine and convoy the magnetic field. The three components (target, magnets, and magnetic yoke) are logged in a stainless steel container. Thus, a tight annular cavity is formed between the interior surface of the outer magnets, the external surface of the central magnet, the lower surface of targets, and the upper surface of the magnetic yoke. This cavity has two holes of $\Phi 6$ mm for two flexible drains to feed and evacuate cooling water, which enters in the cathode through the inlet pipe

and circulates the cavity to extract the heat generated in the target and magnets and leaves through the outlet pipe.

3 Mathematical modeling

3.1 Governing equations

To study characteristics of the cooling effect on the target at different inlet velocities and heat fluxes, the governing equations of continuity, momentum, and energy are expressed as follows [17, 18]:

$$\nabla(\rho \vec{v}) = S_m, \tag{1}$$

where S_m is the mass added to the continuous phase from the dispersed second phase and any user-defined sources.

$$\nabla(\rho \vec{v}\vec{v}) = -\nabla p + \nabla(\overline{\overline{\tau}}) + \rho \vec{g} + \vec{F}, \tag{2}$$

where p is the static pressure, $\overline{\overline{\tau}}$ is the stress tensor, $\rho \vec{g}$ is the gravitational body force, and $\vec{F}$ is the external body forces.

$$\nabla(\vec{v}(\rho E + p)) = \nabla\left(k_{\mathrm{eff}}\nabla T + \left(\overline{\overline{\tau}}_{\mathrm{eff}}\vec{v}\right)\right) + S_h, \tag{3}$$

where k_{eff} is the effective conductivity; the first two terms on the right-hand side are energy transfers due to conduction and viscous dissipation, respectively; and S_h is the volumetric heat sources.

3.2 Turbulence model

Two-equation turbulence models allow the determination of both turbulent length and timescale by solving two separate transport equations. The standard k–ε model in ANSYS FLUENT falls within this class of models and has become the workhorse of practical engineering flow calculations since it was proposed by Launder and Spalding.
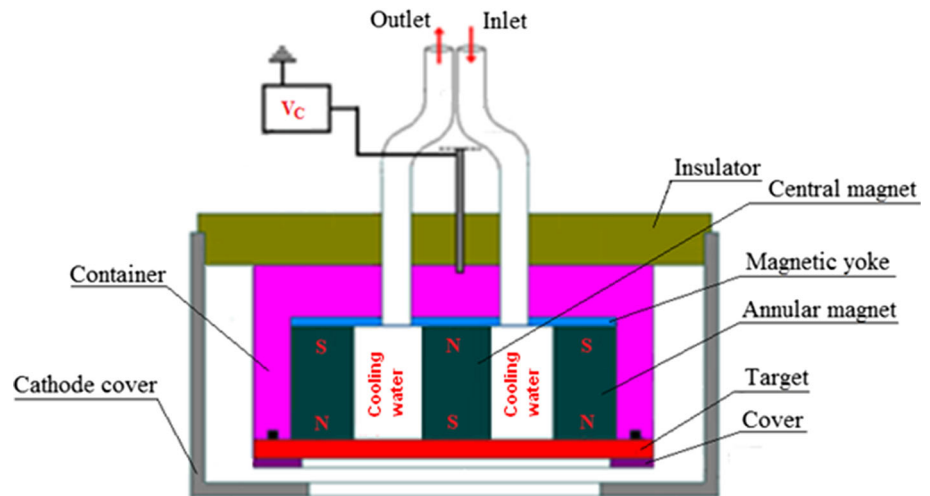
The turbulence kinetic energy, k, and its rate of dissipation, ε, are obtained from the following transport equations [17, 19]:

$$\frac{\partial}{\partial t}(\rho k) + \frac{\partial}{\partial x_i}(\rho k u_i) = \frac{\partial}{\partial x_j}\left[\left(\mu + \frac{\mu_t}{\sigma_k}\right)\frac{\partial k}{\partial x_j}\right] + G_k + G_b$$
$$- \rho\varepsilon - Y_M + S_k, \tag{4}$$

and

$$\frac{\partial}{\partial t}(\rho\varepsilon) + \frac{\partial}{\partial x_i}(\rho\varepsilon u_i) = \frac{\partial}{\partial x_j}\left[\left(\mu + \frac{\mu_t}{\sigma_\varepsilon}\right)\frac{\partial \varepsilon}{\partial x_j}\right]$$
$$+ C_{1\varepsilon}\frac{\varepsilon}{k}(G_k + C_{3\varepsilon}G_b) - C_{2\varepsilon}\rho\frac{\varepsilon^2}{k} + S_\varepsilon, \tag{5}$$

Fig. 1 (Color online) Schematic cross section of the planar-balanced magnetron cathode

where G_k is the generation of turbulence kinetic energy due to the mean velocity gradients, calculated as described in modeling turbulent production in the k–ε models; G_b is the generation of turbulence kinetic energy due to buoyancy, calculated as described in effects of buoyancy on turbulence in the k–ε models; Y_M is the contribution of the fluctuating dilatation in compressible turbulence to the overall dissipation rate, calculated as described in effects of compressibility on turbulence in the k–ε models; $C_{1\varepsilon}$, $C_{2\varepsilon}, C_{3\varepsilon}$ and C_μ are constants; σ_k and σ_ε are the turbulent Prandtl numbers for k and ε, respectively; and S_k and S_ε are user-defined source terms.

The turbulent (or eddy) viscosity is computed as follows:

$$\mu_t = \rho C_\mu \frac{k^2}{\varepsilon}. \tag{6}$$

4 Numerical solution

4.1 Model and grid systems

The MC cooling water passes through a soft iron plate in Φ6 mm pipes and flows into the space interposed between the two magnets which lead to the titanium or nickel target. For the numerical simulation, after designing and drawing the MC using Solidworks 3D CAD software, we adopted the commercial CFD simulation code ANSYS FLUENT (version 14.5) as CFD approach. For perfect reliability of the results, an extensive test for the confirmation of grid independence of the model was carried out by increasing the mesh density and adopting various mesh grading until further refinement showed a difference of less than 1% in two consecutive sets of results [19] (Fig. 2). Given the

geometry simplicity, and to enable saving mesh elements and reduce the error, the choice has been made on the structured grid contained 2,405,001 quad nodes and 2,301,728 elements. A 3D steady-state numerical model of heat transfer with four resolutions to ensure mesh independence is adopted. The problem is processed as a single-phase turbulent flow.

4.2 Numerical method and boundaries conditions

In this paper, the turbulence phenomena are described by a classical standard k–ε model in combination with "standard wall treatment" for the near-wall treatment; the value of y^+ between 1.5 and 5.17, as appropriate, is considered reasonable for the selected near-wall treatment approach. The choice of these models was based on their large citations in literature devoted to this domaine, and on the several tests of convergence by combining different models of turbulence. Table 1 lists correlated information for the numerical study.

The Ti and Ni targets were numerically analyzed at cooling velocities of 0.01, 0.05, and 0.1 m/s, each at heat fluxes of 12,738 and 25,476 W/m^2 (totaling 12 simulations). We used the CFD code ANSYS FLUENT 14.5 to simulate the flow around the target. The equations governing the flows were discretized with the finite volume method (FVM) which is well suited for simulating various types of conservation laws. The SIMPLEC algorithm (semi-implicit method for pressure-linked equations-consistent) was used to solve the Navier–Stokes equations. The standard k–ε model was used to analyze the turbulent flow. For a better accuracy, no-slip boundary conditions for velocity at the walls were assumed. The boundary conditions for the simulation are given in Table 2, and material properties in Table 3.

Fig. 2 (Color online) Meshing of the coolant inside magnetron cathode
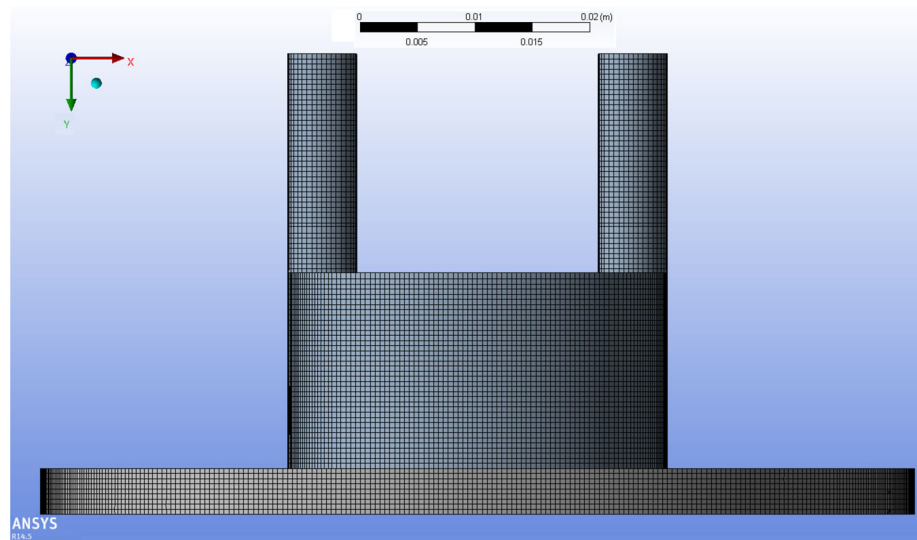
Table 1 Magnetron cathode numerical model input

Models		Status
Solver	Time	Steady
	Type	Pressure based
	Velocity formulation	Absolute
	Gravity (Y-direction)	-9.81 m/s^2
Models	Energy	Active
	Multiphase	Off
	Viscous	Standard k–ε
	Near-wall treatment	Standard
Solution methods	Scheme	SIMPLEC
	Gradient	Least square cell based
	Pressure	Standard
	Momentum	Second-order upwind
	Turbulent kinetic energy	First-order upwind
	Turbulent dissipation rate	First-order upwind
	Energy	Second-order upwind

Table 2 Initial conditions

Parameters	Values
Inlet velocity (m s^{-1})	0.01, 0.05, 0.1
Inlet water temperature (K)	303.15
Wall heat flux (W m^{-2})	12,738, 25,476
Pressure (Pa)	1,001,325

5 Results and discussion

The temperature contours and axial temperature profiles (Fig. 3) show that the Ni and Ti target temperatures at local positions can exceed the Curie temperatures of the magnets used.

At the flow velocity of 0.01 m/s and heat density of 25,476 W/m^2, the Ti and Ni targets reached maximum temperatures of 509 and 482 K, respectively, in the surrounding area of the outlet water orifice. At 0.05 m/s and 25,476 W/m^2, the target temperatures were favorable to have an appropriate sputtering yield but still above the optimal functional temperature of the magnets. Then, 0.1 m/s is an improvement flow velocity for cooling of the sensitive components of the magnetron cathode, with maximum temperatures of the Ti and Ni targets being 347 and 338 K, respectively. The temperatures can be decreased more by heat dissipation between the cathode and sputtering chamber.

Figure 4 shows the velocity streamlines of the cooling water path in the embedded blank between the two magnets and the target at flow rate of 0.1 m/s. The cooling fluid was
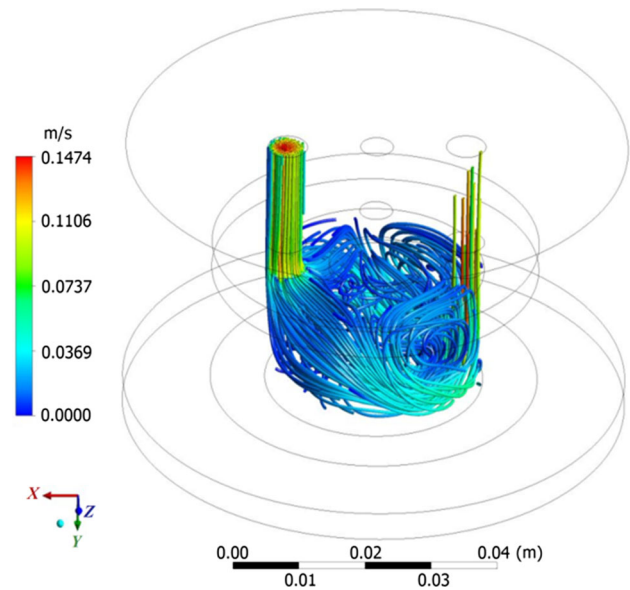
Table 3 Material properties

Properties	Water	Ti	Ni
Density (kg m^{-3})	998.2	4500	8900
Specific heat (J kg^{-1} K^{-1})	4182	523	460.6
Thermal conductivity (W m^{-1} K^{-1})	0.6	21.9	91.74
Viscosity (10^{-6} kg m^{-1} s^{-1})	1003	–	–

roughly slow moving close to the contact surfaces of the peripheral magnet, and the outside surfaces of central magnets were under supplied. Clearly, boundary layers were growing in near-surface regions. This is a result of the momentum exchange occurred between the mainstream fluid and coolant in the shear layer.

The results show that for increasing power supply of the cathode, the inlet coolant temperature should be decreased; otherwise, the sensitive components would attain the functional temperature limit. An improvement in the cathode design is necessary for depositing thin films with high powers. It is suggested that this improvement may be done by increasing the volume of the embedded blank, by changing the flow path inside the cathode, and by improving the heat dissipation.

These can be done by:

1. Enlarging the annular cavity of circulation of cooling water in contact with permanent magnets by reducing thickness of the stainless steel container and/or

Fig. 4 (Color online) Velocity streamlines of the coolant water path in magnetron cathode

diameter of the central permanent magnet, and thickness of the annular permanent magnet, while preserving the magnetic field intensity and the configuration of magnetic field lines;

2. Modifying the inlet and outlet sections of cooling water into a divergent or convergent section, instead of the uniform circular section;
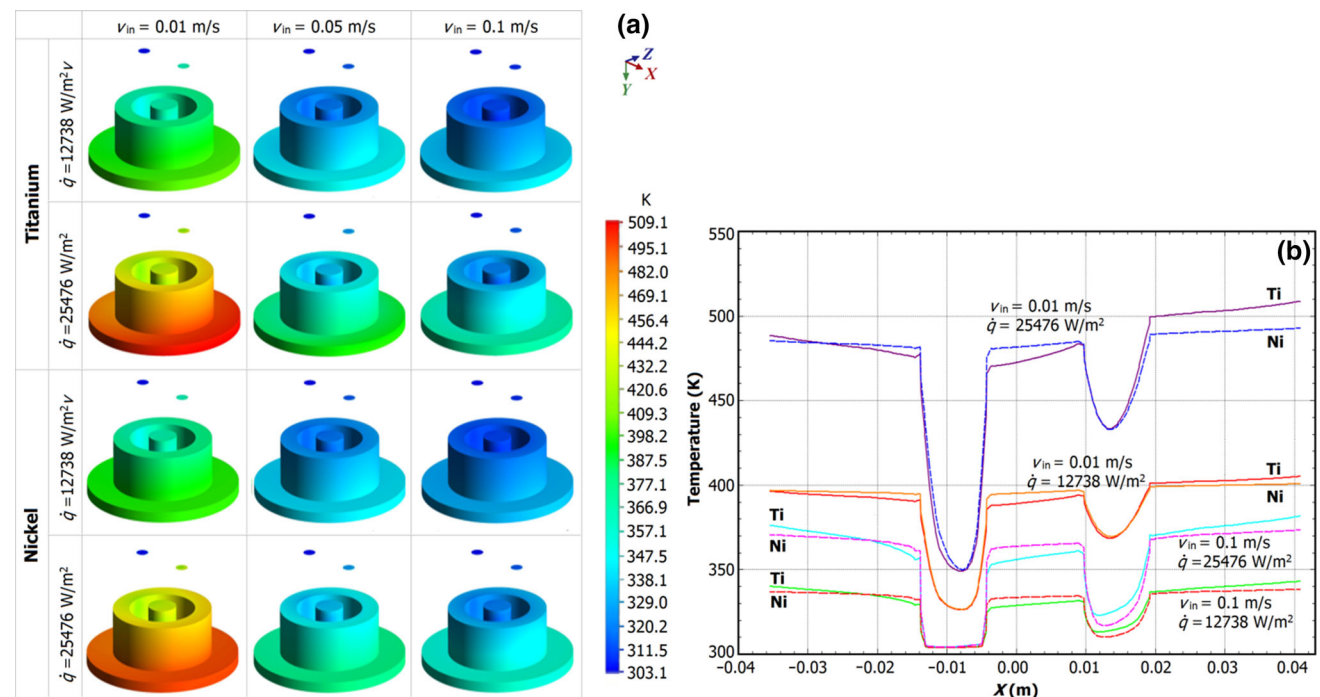
Fig. 3 (Color online) 3D temperature contours (**a**) and axial profile (**b**) of Ti and Ni targets at different inlet coolant velocities and heat flux densities

3. Using compatible materials with good thermal conductivity, in particular the material of the container of the cathode;

4. Reducing the target area and optimizing the cathode–anode distance; and

5. Connecting only the target to the power supply, not to the container, magnetic yoke, and target cover.

6 Conclusion

The cooling effect on nickel and titanium targets and permanent magnets in dual cathode magnetron sputtering system was simulated at different water coolant inlet velocities and power densities. The results show that the magnets reached Curie temperature, and the temperature of both targets rises abruptly at low inlet velocity and high power density. At flow velocity of 0.1 m/s, an improvement in cooling of the sensitive components was observed. Flow path of cooling water allowed to evidence that there was roughly slow moving and undersupplied area. Parametric study will be done to further enhance heat removal from magnetron cathode and overcome cooling deficiencies at high power density, considering the cathode design, thermal hydraulic parameters of the coolant water, thermal gradient and mechanical deflections, sputtering conditions, and quality of the obtained thin films.

References

1. K. Wasa, S. Hayakawa, *Handbook of Sputter Deposition Technology: Principles, Technology and Application* (Noyes Publications, Park Ridge, 1992)
2. P.J. Kelly, R.D. Arnell, Magnetron sputtering: a review of recent developments and applications. Vacuum **56**(3), 159–172 (2000). doi:10.1016/S0042-207X(99)00189-X
3. S.M. Rossnagel, J.J. Cuomo, W.D. Westwood, *Westwood, Handbook of Plasma Processing Technology Fundamentals. Etching, Deposition and Surface Interactions* (Noyes Publications, Park Ridge, 1990)
4. R.K. Waits, Planar magnetron sputtering. J. Vac. Sci. Technol. (1978). doi:10.1116/1.569451
5. R.S. Rastogi, V.D. Vankar, K.L. Chopra, Simple planar magnetron sputtering source. Rev. Sci. Instrum. (1987). doi:10.1063/1.1139388
6. C. Christou, Z.H. Barber, Ionization of sputtered material in a planar magnetro discharge. J. Vac. Sci. Technol. **18**(6), 2897–2907 (2000). doi:10.1116/1.1312370
7. C.A Bishop, Magnetron sputtering source design options, in *Vacuum Deposition Onto Webs, Films and Foils* (William Andrew Publishing, Norwich, 2015), pp 401–412
8. A.S. Peter, R.K. Milan, A. Terry, *US patent 5407551, Planar Magnetron Sputtering Apparatus* (Pleasant Hill, Trumbly, 1995)
9. E.D. Richard, H. Manuel, M. San et al., US patent 5603816, Sputtering device and target with cover to hold cooling fluid (1997)
10. Y. Kusumoto, Inverse problem in planar magnetron sputtering. J. Appl. Phys. (1997). doi:10.1063/1.366282
11. M.R. Lake, G.L. Harding, Cathode cooling apparatus for a planar magnetron sputtering system. J. Vac. Sci. Technol. **A2**, 1391 (1984). doi:10.1116/1.572372
12. H. Takatsuji, S. Tsuji, K. Kuroda et al., The influence of cooling water flowing in the sputtering target on aluminum based thin film nanostructure deposited on glass substrates. Thin Solid Films **343**(344), 465–468 (1999). doi:10.1016/S0040-6090(98)01677-0
13. J.S. Baik, Y.J. Kim, A study of the heat transfer enhancement in *Magnetron Sputtering System. ASME/JSME 2007 Thermal Engineering Heat Transfer Summer Conference,* vol. 1 (Vancouver, British Columbia, Canada, July 8–12, 2007). doi: 10.1115/HT2007-32182
14. R.P. Doerner, S.I. Krasheninnikov, K. Schmid, Particle-induced erosion of materials at elevated temperature. J. Appl. Phys. **95**, 4471–4475 (2004). doi:10.1063/1.1687038
15. A. Caillard, M. El'Mokh, N. Semmar et al., Energy transferred from a hot nickel target during magnetron sputtering. IEEE Trans. Plasma Sci. **42**(10), 2802–2803 (2014). doi:10.1109/TPS.2014.2338742
16. M. Salhi, S. E. H. Abaidia, Algeria patent 140171, Système de pulvérisation bi-cathodes magnétrons (2014)
17. Fluent 14.5.0. Fluent user's guide. USA: ANSYS, Inc (2012)
18. A. Shahmohammadi, A. Jafari, Application of different CFD multiphase models to investigate effects of baffles and nanoparticles on heat transfer enhancement. Front. Chem. Sci. Eng. **8**(3), 320–329 (2014). doi:10.1007/s11705-014-1437-7
19. B. Mohamedi, S. Hanini, A. Ararem et al., Simulation of nucleate boiling under ANSYS-FLUENT code by using RPI model coupling with artificial neural networks. Nucl. Sci. Tech. **26**(4), 040601 (2015). doi:10.13538/j.1001-8042/nst.26.040601